Available online at www.sciencedirect.com

ScienceDirect

Journal of Ocean Engineering and Science 2 (2017) 268–278

www.elsevier.com/locate/joes

Numerical study of vibrations of a vertical tension riser excited at the top end

Bowen Fu, Decheng Wan*

State Key Laboratory of Ocean Engineering, School of Naval Architecture, Ocean and Civil Engineering, Shanghai Jiao Tong University, Collaborative Innovation Center for Advanced Ship and Deep-Sea Exploration, Shanghai 200240, China

Received 15 May 2017; received in revised form 11 August 2017; accepted 6 September 2017
Available online 14 September 2017

Abstract

This paper presents numerical simulations of vortex-induced vibrations of a vertical riser which is sinusoidally excited at its top end in both one and two directions in still water. A computational fluid dynamics method based on the strip theory is used. The riser's responses to both top-end and two-end excitations are carefully examined. In low reduced velocity cases, the in-line vibrations consist of three components, the low-frequency oscillation, the first-natural-frequency vibration during the riser reversal, and the second-natural-frequency vibration due to vortex shedding. The sheared oscillatory flow along the span causes low-frequency oscillations in higher modes in the in-line direction, thus forming 'X' shaped, 'II' shaped, and 'O' shaped trajectories at various positions along the span when the riser is excited at its top end in one direction. In the presence of excitations in the other direction, more complex trajectories appear.

© 2017 Shanghai Jiaotong University. Published by Elsevier B.V.
This is an open access article under the CC BY-NC-ND license. (http://creativecommons.org/licenses/by-nc-nd/4.0/)

Keywords: Vortex-induced vibration; Oscillatory flow; Riser; Platform motion; Viv-FOAM-SJTU solver.

1. Introduction

Marine risers can experience vortex-induced vibrations (VIV) when exposed to currents. Furthermore, offshore floating platforms subject to waves, currents or winds may cause risers to reciprocate. Risers are thus exposed to a relatively oscillatory flow with a degree of shear and forced to cross their own wakes, rendering their responses more like wake-induced vibrations. The vortex shedding frequencies keep going up and down due to the continuous flow velocity changes. Lock-in or resonance phenomena occur when the vortex shedding frequencies meet one of risers' natural frequencies.

Vibrations of rigid cylinders in oscillatory flow have been the subject of numerous investigations in the past several decades [1,2]. A comprehensive review of the early investigations can be found in Sumer and Fredsøe [3]. More investigations of vibrations of rigid cylinders in oscillatory flow have been conducted in recent years. Zhao et al. [4,5] conducted two-dimensional numerical studies of vibrations of a circular cylinder in oscillatory flow and combined steady and oscillatory flow. Fernandes et al. [6] experimentally investigated various trajectories of a cylinder in oscillatory flow.

Vortex-induced vibrations of flexible cylinders in oscillatory flow have received more and more attention. Duggal and Niedzwecki [7] conducted a large-scale experimental study of vibrations of a long flexible cylinder in regular waves. Anagnostopoulos and Iliadis [8] used a finite element technique to study the in-line response of a flexible cylinder in oscillatory flow. Park et al. [9,10] and Senga and Koterayama [11] conducted experimental and numerical studies on vibrations of a hanging riser subject to regular or irregular top-end excitations. Riveros et al. [12] experimentally and numerically studied a model riser sinusoidally excited at its top end. More recently, Fu et al. [13] and Wang et al. [14] conducted model tests on vibrations of a flexible cylinder in oscillatory flow. Thorsen at al. [15] improved their semi-empirical method to predict cross-flow VIV of a flexible cylinder in oscillatory flow.

---

* Corresponding author.
E-mail address: dcwan@sjtu.edu.cn (D. Wan).

http://dx.doi.org/10.1016/j.joes.2017.09.001

2468-0133/© 2017 Shanghai Jiaotong University. Published by Elsevier B.V. This is an open access article under the CC BY-NC-ND license. (http://creativecommons.org/licenses/by-nc-nd/4.0/)

Most of the previous numerical studies of risers in oscillatory flow are based on semi-empirical methods, and studies based on computational fluid dynamics (CFD) methods are lacking, which can better reveal interactions between the flow and the riser. In the present work, vibrations of a vertical top-tensioned riser sinusoidally excited at its top end are numerically investigated using a CFD method based on strip theory. The simulations are conducted by the in-house solver viv-FOAM-SJTU, which has been validated in previous studies [16,17]. The present article is organized as follows. Key points to be considered in the simulations are introduced at first. Then the capability of the solver to handle the vibrations of flexible cylinders in oscillatory flow is further validated. And simulation results of vibrations of a riser excited at its top end in one and two directions are carefully examined in a later section.

2. Method

The incompressible Reynolds-averaged Navier–Stokes equations are solved numerically to obtain the hydrodynamic forces acting on the riser. The SST $k-\omega$ turbulence model is employed to determine the Reynolds stresses. Considering the large scale in the axial direction of the flow domain, two-dimensional flow strips positioned equidistantly along the span are computed instead of the entire three-dimensional flow field. As Willden and Graham [18] has mentioned, though three-dimensional vortices may develop, an effect of lock-in actually maintains the locally two-dimensional property, making it appropriate to compute the fluid dynamics locally in a two-dimensional way. Hydrodynamic forces at any positions along the span can be interpolated accordingly. The number of simulation strips can be determined by considering the highest mode of vibration. Three strips are required per half wave-length of vibration [18]. The highest mode considered in the present work is the 5th mode. As a result, 20 strips seem sufficient for the simulation. The PIMPLE algorithm in the OpenFOAM is used to compute the two-dimensional flow fields.

In numerical simulations, the top end or two ends of the riser are forced to oscillate sinusoidally. The excitation motion of the riser is a periodic function of time, expressed as

$$x_s = A \cdot \sin\left(2\pi t \cdot T_w^{-1}\right), \tag{1}$$

$$u_s = 2\pi A \cdot T_w^{-1} \cdot \cos\left(2\pi t \cdot T_w^{-1}\right), \tag{2}$$

A being the excitation amplitude, T_w the excitation period, x_s the excitation displacement and u_s the excitation velocity. Reduced velocity U_r and its maximum value $U_{r\ max}$ can be written as

$$U_r = \frac{u_s}{f_{n1}D} = \frac{2\pi A}{T_w f_{n1}D} \cos\left(2\pi t \cdot T_w^{-1}\right) \tag{3}$$

$$U_{r\ max} = \frac{u_{s\ max}}{f_{n1}D} = \frac{2\pi A}{T_w f_{n1}D}, \tag{4}$$

where f_{n1} is the first natural frequency of the riser. In the sinusoidal flow, the Keulegan–Carpenter (KC) number can be expressed as

$$KC = u_{s\ max} T_w \cdot D^{-1} = 2\pi A \cdot D^{-1}, \tag{5}$$

in which $u_{s\ max}$ is the maximum excitation velocity.

Thus, the riser's total displacement x_t at any positions along the span can be expressed in terms of the quasi-static component due to support motion x_s, and the deflections of the riser from its straight-line condition x [19]:

$$x_t = x_s + x. \tag{6}$$

The quasi-static displacement x_s is linear along the span for riser pinned at the two ends. More details about obtaining quasi-static displacements can be found in Clough and Penzien [19]. The equilibrium of forces for this system can be written as

$$f_I + f_D + f_S = f_{Hx}, \tag{7}$$

where f_I, f_D, f_S, f_{Hx} are the inertial, the damping, the spring, and the hydrodynamic forces in the corresponding direction, respectively. The force components can be expressed as $f_I = m\ddot{x}_t$, $f_D = c\dot{x}$, $f_S = kx$, m, c, k being the mass, the damping and the stiffness of the system. Thus we have

$$m\ddot{x}_t + c\dot{x} + kx = f_{Hx}, \tag{8}$$

$$m\ddot{x} + c\dot{x} + kx = f_{Hx} - m\ddot{x}_S. \tag{9}$$

With the riser modeled as a small displacement Bernoulli–Euler bending beam and two ends set as pinned, we have

$$\underbrace{m\frac{\partial^2 x_t(z,t)}{\partial t^2}}_{m\ddot{x}_t} + \underbrace{c\frac{\partial x(z,t)}{\partial t}}_{c\dot{x}} + \underbrace{EI\frac{\partial^4 x(z,t)}{\partial z^4} - \frac{\partial\left[T(z)\frac{\partial x(z,t)}{\partial z}\right]}{\partial z}}_{kx} = f_{Hx}(z,t) \tag{10}$$

$$\underbrace{m\frac{\partial^2 x(z,t)}{\partial t^2}}_{m\ddot{x}} + \underbrace{c\frac{\partial x(z,t)}{\partial t}}_{c\dot{x}} + \underbrace{EI\frac{\partial^4 x(z,t)}{\partial z^4} - \partial\underbrace{\left[T(z)\frac{\partial x(z,t)}{\partial z}\right]}_{\partial z}}_{kx} = f_{Hx}(z,t) - m\underbrace{\frac{\partial^2 x_s(z,t)}{\partial t^2}}_{m\ddot{x}_S} \tag{11}$$

where flexural stiffness EI and linear density m keep constant along the span, while tension $T(z)$ varies along the span due to gravity. This also applies to the cross-flow displacement. In the finite element method, the equations can be discretized as

$$\mathbf{M}\ddot{\mathbf{x}} + \mathbf{C}\dot{\mathbf{x}} + \mathbf{K}\mathbf{x} = \mathbf{f}_{Hx} - \mathbf{M}\ddot{\mathbf{x}}_{\mathbf{S}}, \tag{12}$$

$$\mathbf{M}\ddot{\mathbf{y}} + \mathbf{C}\dot{\mathbf{y}} + \mathbf{K}\mathbf{y} = \mathbf{f}_{Hy} - \mathbf{M}\ddot{\mathbf{y}}_{\mathbf{s}}, \tag{13}$$

where $\mathbf{x}$, $\mathbf{x_s}$, $\mathbf{y}$, and $\mathbf{y_s}$ are nodal displacement vectors, $\mathbf{M}$, $\mathbf{C}$, $\mathbf{K}$ are the mass, the damping and the stiffness matrices, and $\mathbf{f}_{Hx}$ and $\mathbf{f}_{Hy}$ are the hydrodynamic force vectors in corresponding directions (including hydrodynamic mass forces). The Rayleigh damping $\mathbf{C} = \alpha\mathbf{M} + \beta\mathbf{K}$ is adopted, where α and β are calculated based on the natural frequencies of two

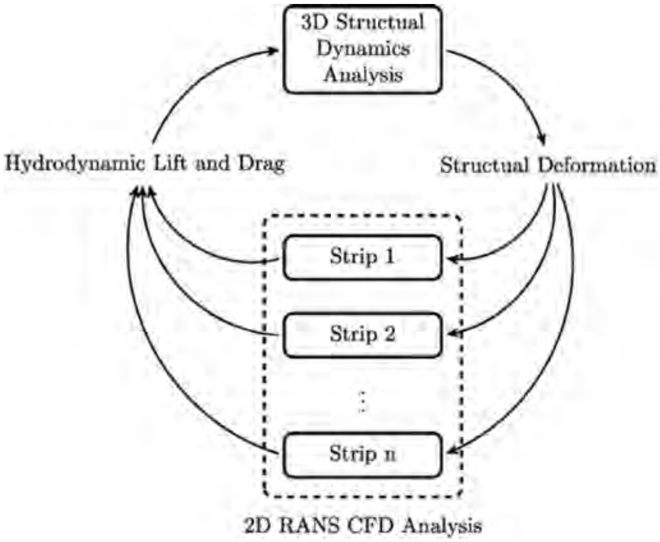

Fig. 1. Fluid-structure interaction.

mainly involved modes, with a damping ratio ζ of 0.03. The equation can be written as

$$\begin{bmatrix}\alpha\\ \beta\end{bmatrix} = \frac{2\zeta}{f_{ni}+f_{nj}}\begin{bmatrix}2\pi f_{ni} f_{nj}\\ 1/(2\pi)\end{bmatrix}. \tag{14}$$

The equations are solved using the Newmark-beta method [19].

The tension variation along the span for a vertical riser is considered in geometric stiffness matrices. The varying tension for each element can be written as $T(z) = T_b + K_T \cdot z$, where T_b is the tension at the element bottom, z denotes distance from the element bottom and $K_T = (m - \rho\pi D^2/4)g$. In the 4 × 4 element geometric stiffness matrix, the element geometric-stiffness coefficients are calculated through $k_{G_{ij}} = \int_0^l T(z)\psi_i'(z)\psi_j'(z)dz$, where $\psi_i'(z)$ is the derivative of shape function $\psi_i(z)$ and l is the length of the element [19]. Thus the following consistent element geometric stiffness matrix can be formed:

$$\begin{bmatrix}
\frac{3K_T}{5}+\frac{6T_b}{5l} & \frac{K_T l}{10}+\frac{T_b}{10} & -\frac{3K_T}{5}-\frac{6T_b}{5l} & \frac{T_b}{10}\\
\frac{K_T l}{10}+\frac{T_b}{10} & \frac{K_T l^2}{30}+\frac{2l}{15}T_b & -\frac{K_T l}{10}-\frac{T_b}{10} & -\frac{K_T l^2}{60}-\frac{lT_b}{30}\\
-\frac{3K_T}{5}-\frac{6T_b}{5l} & -\frac{3K_T}{5}-\frac{6T_b}{5l} & \frac{3K_T}{5}+\frac{6T_b}{5l} & -\frac{T_b}{10}\\
\frac{T_b}{10} & -\frac{K_T l^2}{60}-\frac{lT_b}{30} & -\frac{T_b}{10} & \frac{K_T l^2}{10}+\frac{2l}{15}T_b
\end{bmatrix}, \tag{15}$$

with K_T being zero for a horizontal cylinder.

At the beginning of the fluid-structure interaction procedure, the hydrodynamic forces are mapped to the structural model elements. Following that the displacements of the riser are computed using the finite element method and passed to the flow fields. The meshes of flow fields on all strips move or deform accordingly. Thus new flow fields can be computed. The hydrodynamic forces acting on the riser can be obtained and a time step is advanced as a result. The procedure is shown in Fig. 1, based on which the solver viv-FOAM-SJTU is formed.

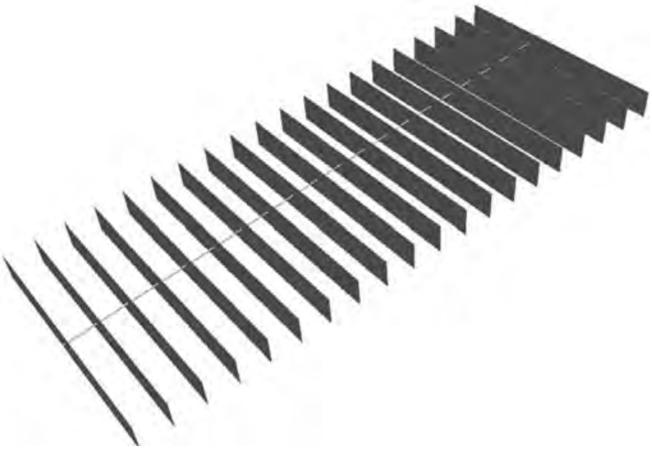

Fig. 2. Twenty strips located equidistantly along the span of the riser.

(a) Initial mesh on each strip;

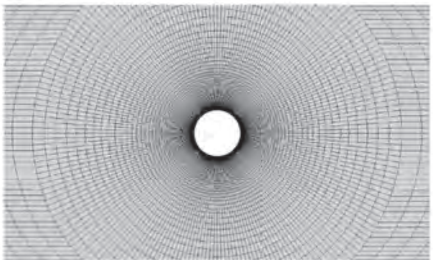

(b) Mesh near the riser on each strip.

Fig. 3. Mesh details on each strip.

Table 1
Main structural properties of the riser.

	Symbols	Values	Units
Mass ratio	m^*	1.53	–
Diameter	D	0.024	m
Bending stiffness	EI	10.5	$\mathrm{N\cdot m^2}$
Top tension	T_t	500	N

Twenty strips equidistantly located along the span of the riser are plotted in Fig. 2. These strips share the same initial flow field mesh, as shown in Fig. 3. Meshes for cases with excitations in two directions are wider in the cross-flow direction. The motion solver “displacementLaplacian” in OpenFOAM is employed to handle the dynamic mesh [20]. Imposed on the surface of the riser is the no-slip boundary, and no external current is present. The riser is discretized into 80 elements, with each element imposed of uniformly distributed loads. Main parameters of the riser are listed in Table 1. Natural frequencies of the riser in still water are calculated using the finite element method with a hydrodynamic mass coefficient of 1. The first few of them are set out in Tables 2 and 3.

Table 2
Calculated natural frequencies of the short riser.

	Symbols	Values	Units
Length	L	4	m
First natural frequency	f_{n1}	2.68	Hz
Second natural frequency	f_{n2}	5.46	Hz

Table 3
Calculated natural frequencies of the long riser.

	Symbols	Values	Units
Length	L	12	m
First natural frequency	f_{n1}	0.86	Hz
Second natural frequency	f_{n2}	1.72	Hz
Third natural frequency	f_{n3}	2.60	Hz
Fourth natural frequency	f_{n4}	3.48	Hz
Fifth natural frequency	f_{n5}	4.38	Hz

Table 4
Main parameters for simulation cases.

Case	L (m)	KC_x	KC_y	$U_{r\ \max}$	$V_{r\ \max}$	Excited at
1	4	84	0	4	0	Two ends
2	4	168	0	30	0	Two ends
3	4	168	0	8	0	Top end
4	12	84	0	12	0	Top end
5	12	84	21	12	6	Top end
6	12	84	42	12	12	Top end

3. Validations

The capability of the solver to predict the vibrations of flexible cylinders in oscillatory flow is validated based on two cases against data from a model test and a simulation using a semi-empirical method. A total of six cases mentioned in the article are shown in Table 4. Symbols KC_x, KC_y, $U_{r\ \max}$ and $V_{r\ \max}$ in the table denote KC numbers and maximum reduced velocities at the top end of the riser in the in-line and cross-flow directions, respectively. Excitations at the two ends are the same and in phase when it is described as ‘excited at two ends’. The model considered in the validation section is a two-end excited flexible horizontal cylinder instead of a top-end excited vertical riser.

3.1. Low reduced velocity case

In case 1, the cross-flow vibrations are mainly in the 1st mode, i.e. one half-wave along the span, due to the low reduced velocities. The largest amplitude of cross-flow vibration occurs at mid-span of the riser. In Fig. 4 the development of the vibration within half an excitation period in both the present simulation and the model test from Wang et al. [14] appears similar. The critical value of $\sqrt{2}/2$ of the maximum cross-flow displacement is used to distinguish the ‘lock-in’ stage from the ‘build-up’ and ‘die-out’ stages. The lock-in duration is 21% of the half excitation period in the simulation, 22% for Wang et al. [14]. The vibration amplitude in the present simulation is slightly larger. Moreover, the vibration in the simulation does not damp as quickly as in the test, rendering the hysteresis effect of the ‘lock-in’ stage with respect to the maximum reduced velocity more evident. The slow damping may be due to the poor selection of damping ratio, which is not given in Wang et al. [14]. Considering that we are comparing a detailed displacement history at a single point on the cylinder rather than a general dominant vibration mode, the simulation agrees reasonably with the test.

3.2. High reduced velocity case

The simulation results of case 2 in Thorsen et al. [15] using a semi-empirical method and the present work are presented in Figs. 5 and 6, respectively. Modal weights of cross-flow displacements in Fig. 6 are obtained through modal decompositions in the least-squares sense [21,22] via

$$\phi^{\mathbf{T}}\phi\mathbf{w_y} = \phi^{\mathbf{T}}\mathbf{y}, \tag{16}$$

where $\mathbf{w_y}$ is the modal weight vector of cross-flow displacements and only those desirable mode shapes are included in the matrix of mode shapes ϕ. Model weights in the other direction can be computed in a similar way. First six mode shapes are shown in Fig. 7.

The KC number and the maximum reduced velocity $U_{r\ \max}$ in Thorsen et al. [15] are 178 and 32, slightly larger than them in the present simulation. Results agree well for the 4th-mode-dominated stage during the first half period and the 3rd-mode-dominated stage during the last half period. The modal weight

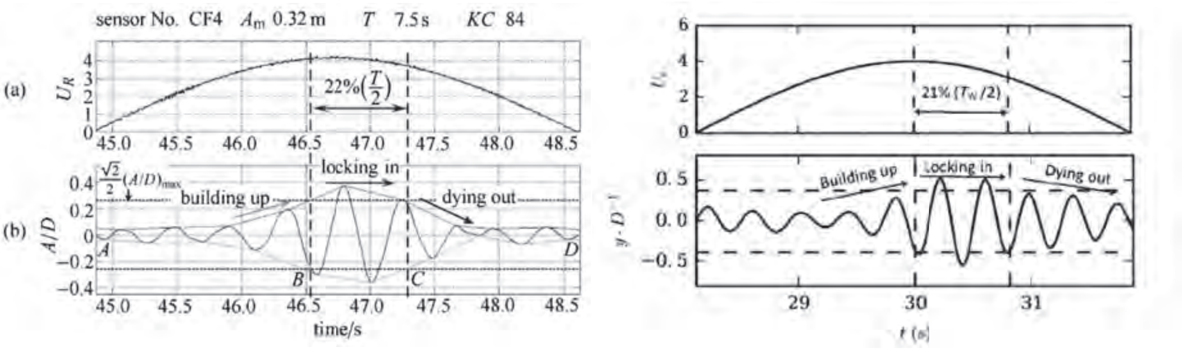

(a) Wang et al. (2014) (b) The present simulations

Fig. 4. Development of the cross-flow vortex-induced vibrations at the mid-span of the riser in case 1 within half an excitation period.

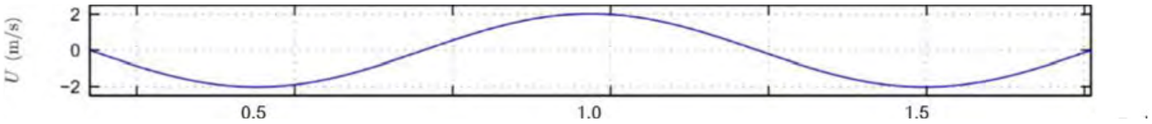

(a) Incoming flow velocity U as a function of time.

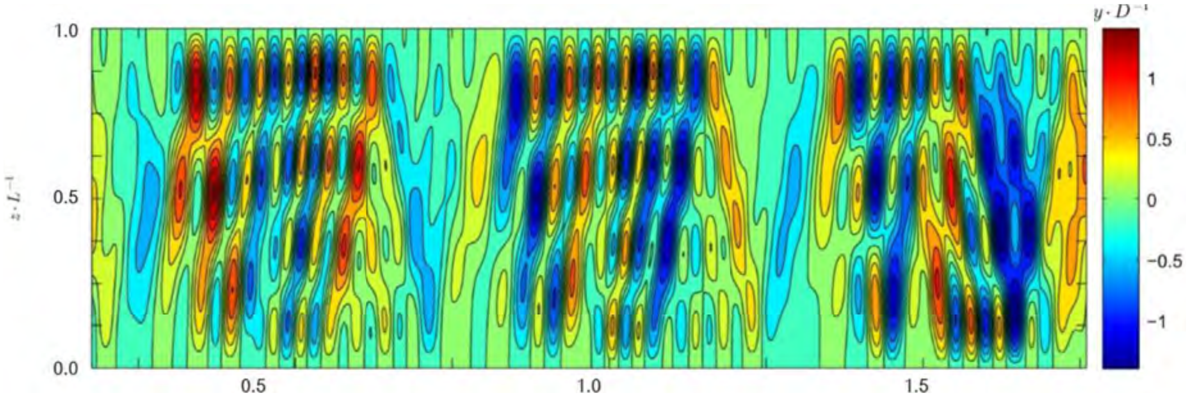

(b) Contour plot of the cross-flow displacement $y \cdot D^{-1}$.

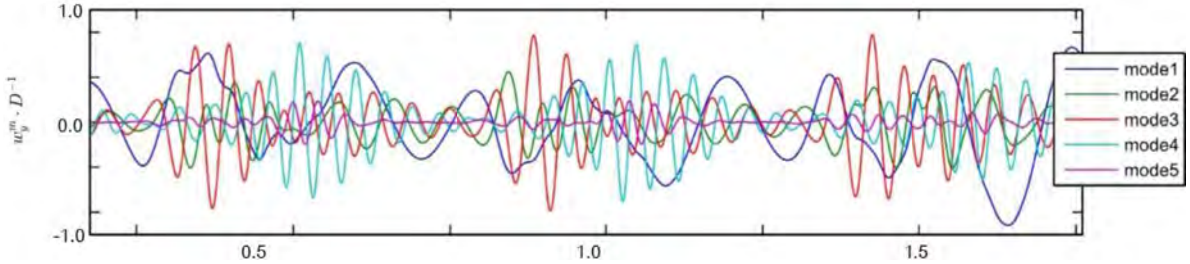

(c) First five modal weights.

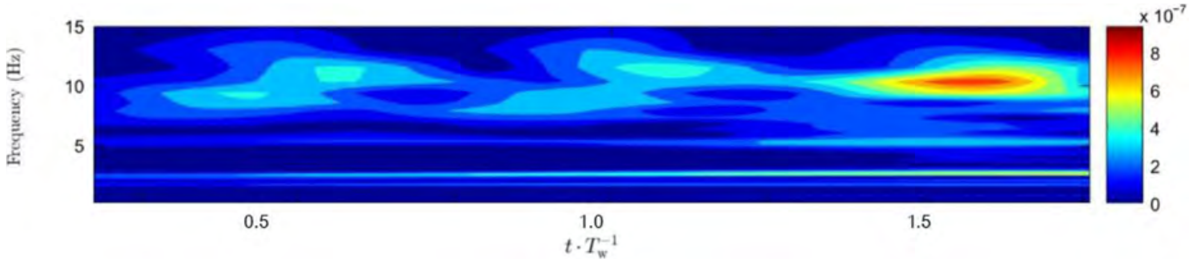

(d) Wavelet contour plot of the cross-flow displacement $y \cdot D^{-1}$ at mid-span of the riser.

Fig. 5. Simulation results of case 2 ($KC = 178$, $U_{r\ max} = 32$) in Thorsen et al. [15].

for the 5th mode is higher in the present simulation. The vibration frequency at mid-span of the riser is also slightly higher. As is known, a reduced velocity $U_{r\ max}$ of 6 will bring out the largest vibration amplitude for the 1st mode, it seems reasonable to suppose that a reduced velocity of 30 will excite the 5th mode significantly, which is more consistent with the present simulation.

4. Results

The time t is non-dimensionalized by the excitation period T_w in the following analyses. Since $x_s = A \cdot \sin(2\pi\ t \cdot T_w^{-1})$, the excitation displacement gets zero when $t \cdot T_w^{-1} = i +$ 0 or 0.5, approaches peaks when $t \cdot T_w^{-1} = i + 0.25$, and approaches valleys when $t \cdot T_w^{-1} = i + 0.75$, where i is some integer.

4.1. Comparison of two-end excitation and top-end excitation

In the case of the top-end excited vertical riser, the angular acceleration due to the support motion is non-zero and the tension varies along the span due to gravity and buoyancy. Depicted in Fig. 8 are modal weights of the in-line displacements in cases 1 and 3. The low-frequency, large-amplitude fluctuation in the 1st modal weight reflects the effect of the

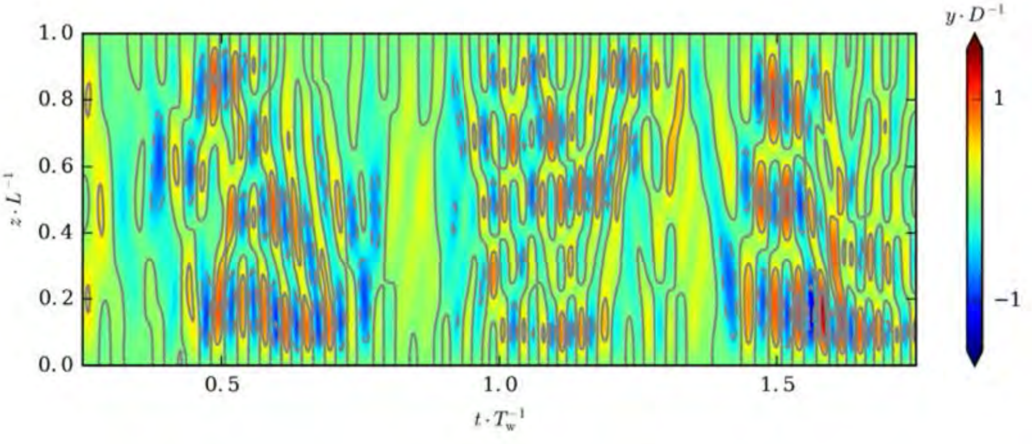

(a) Contour plot of the cross-flow displacement $y \cdot D^{-1}$.

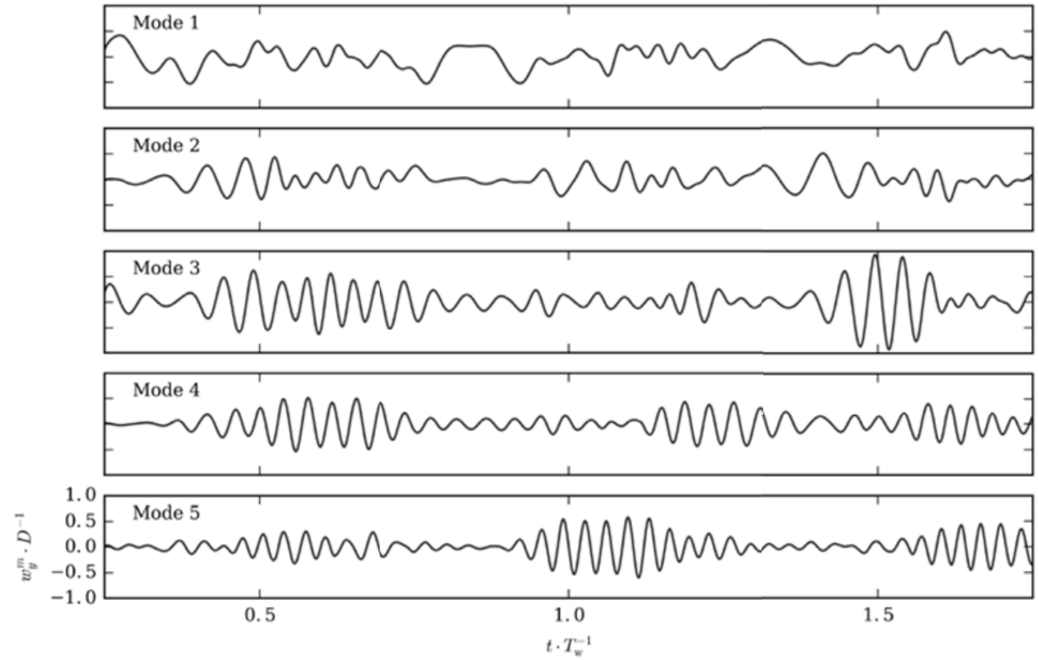

(b) First five modal weights.

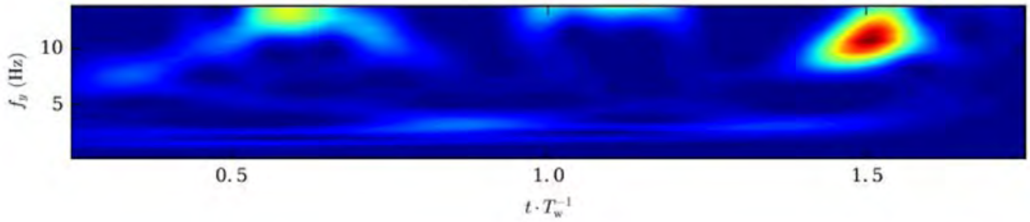

(c) Wavelet contour plot of the cross-flow displacement $y \cdot D^{-1}$ at mid-span of the riser.

Fig. 6. Simulation results of case 2 ($KC = 168$, $U_{r\ \max} = 30$) in the present work.

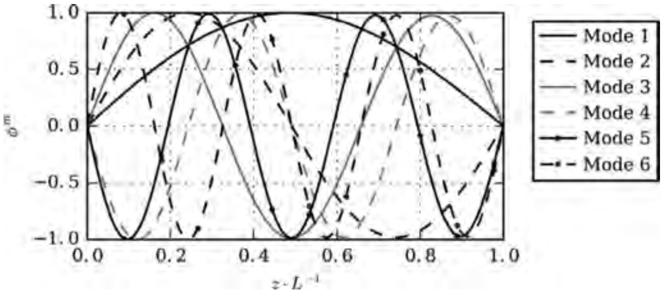

Fig. 7. First six mode shapes.

drag forces. The distinct short-duration intense oscillations in the 1st modal weight are found to be during the riser reversal. Fig. 9 plots the development of the vortices in the plane at mid-span of the riser during this period. The figure shows exactly how the vortices attached on the reversing riser are washed over to the other side, which gives rise to the short-duration oscillations. The oscillations are exactly at the 1st natural frequency. The third component of the in-line displacement is the 2nd modal vibration during lock-in stage. These components are shared by cases 1 and 3. However, the low-frequency oscillation also exists in the 2nd modal weight for case 3. This can be attributed to the shear velocity nature of the oscillatory flow when the riser is excited at only the top end. The drag forces along the riser as a whole contribute to the low-frequency component in the 1st mode, while the difference value between the drag forces of the upper part and the lower part contributes to the low-frequency component in the 2nd mode. That is to say, the drag forces on the upper part of the riser act to excite the 2nd modal component while that of the lower part serve to damp the component. This low-frequency component will further exist in higher modes in excitation directions.

The build-up–lock-in–die-out cycle features can be clearly observed in the cross-flow modal weights in Fig. 10 for both cases. The 1st modal weight for the case 3 is smaller and its 2nd mode is more evident. It is worth noting that the upper part of the riser experiences higher-speed currents and consequently higher vortex shedding frequencies and more energetic excitations, which has the effect of inducing the riser to vibrate at higher frequencies and in higher modes.

The relative trajectories of the vibrations within an excitation period are plotted in Fig. 11. They are viewed from a reference frame which moves with the straight riser axis, i.e. no support motions are included in them; only deflections are reflected in the trajectories. The most intense vibrations in both directions occur during lock-in stages when the in-line deflections reach their extreme values, forming two ‘wings’ at two sides of the trajectories in case 1. The butterfly-shaped trajectory characteristic can be a key feature for low-mode vibrations of flexible cylinders excited at the two ends. Trajectories are different for risers excited at the top end. It has been discussed that the difference of value between the drag forces of the upper part and the lower part of the riser contributes to the low-frequency 2nd modal weights. The 2nd mode forms opposite phases in the in-line displacement for $z \cdot L^{-1} = 0.25,\ 0.75$, the peak and valley of the mode shape and also almost no in-line vibrations during lock-in stages for $z \cdot L^{-1} = 0.5$, the standing point of the mode. All the three positions are in phase for the 1st modal cross-flow vibrations, thus the riser has different trajectories at different positions, i.e. ‘X’ shaped, ‘II’ shaped and ‘O’ shaped trajectories due to various phase differences between the in-line and cross-flow displacements. The ‘in-phase’ 1st modal vibrations in both in-line and cross-flow directions form fundamental trajectories for the riser as in the left part of Fig. 11, while the non ‘in-phase’ 2nd modal vibrations (mainly the in-line low-frequency component) cause variations based on the fundamental trajectories, thus forming the resultant trajectories in the right part of Fig. 11 for the top-end excited riser. The feature is only obvious when the reduced velocity is low. More research should be conducted to explain why it is ‘O’ shaped trajectory for $z \cdot L^{-1} = 0.75$ and ‘X’ for $z \cdot L^{-1} = 0.25$ rather than the opposite.

4.2. Comparison of excitations in one and two directions

In Figs. 12 and 13 are plotted the relative and actual trajectories of cases 4, 5 and 6, respectively. When the riser is excited in two directions, the frequency of the cross-flow excitation is twice that of the in-line excitation, thus forming a ‘∞’ -shaped trajectory shown in Fig. 13. An interesting ‘helmet’ shaped relative trajectory is found in cases 5 and 6. The modal weights in the in-line direction increase considerably

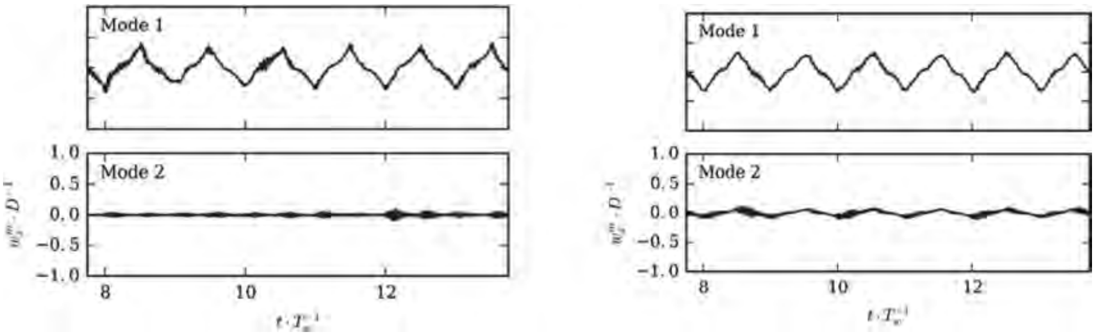

Fig. 8. Time series of modal weights of the in-line displacements $x \cdot D^{-1}$ of cases 1 (left) and 3 (right), $w_x^m \cdot D^{-1}$.

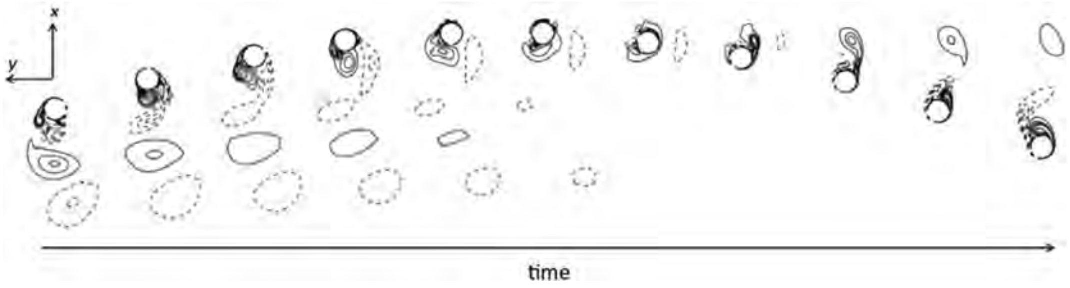

Fig. 9. Development of vortices in the course of riser reversal in the strip at mid-span of the riser in case 1.

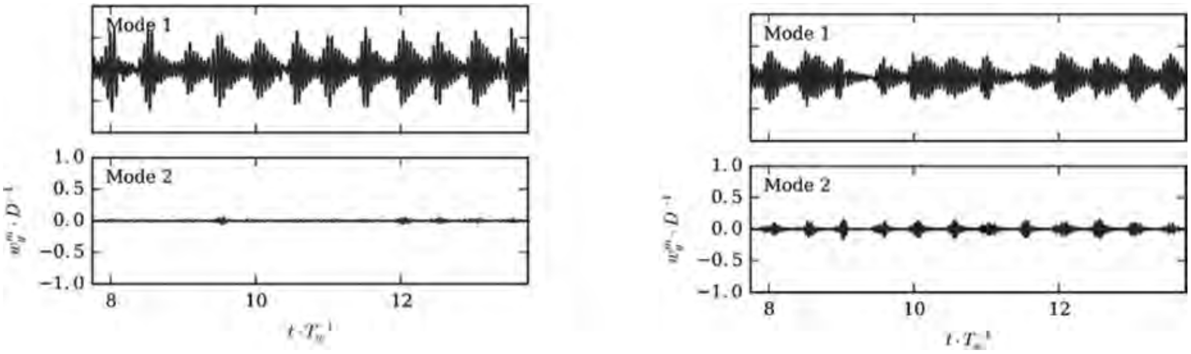

Fig. 10. Time series of modal weights of the cross-flow displacements $y \cdot D^{-1}$ in cases 1 (left) and 3 (right), $w_y^m \cdot D^{-1}$.

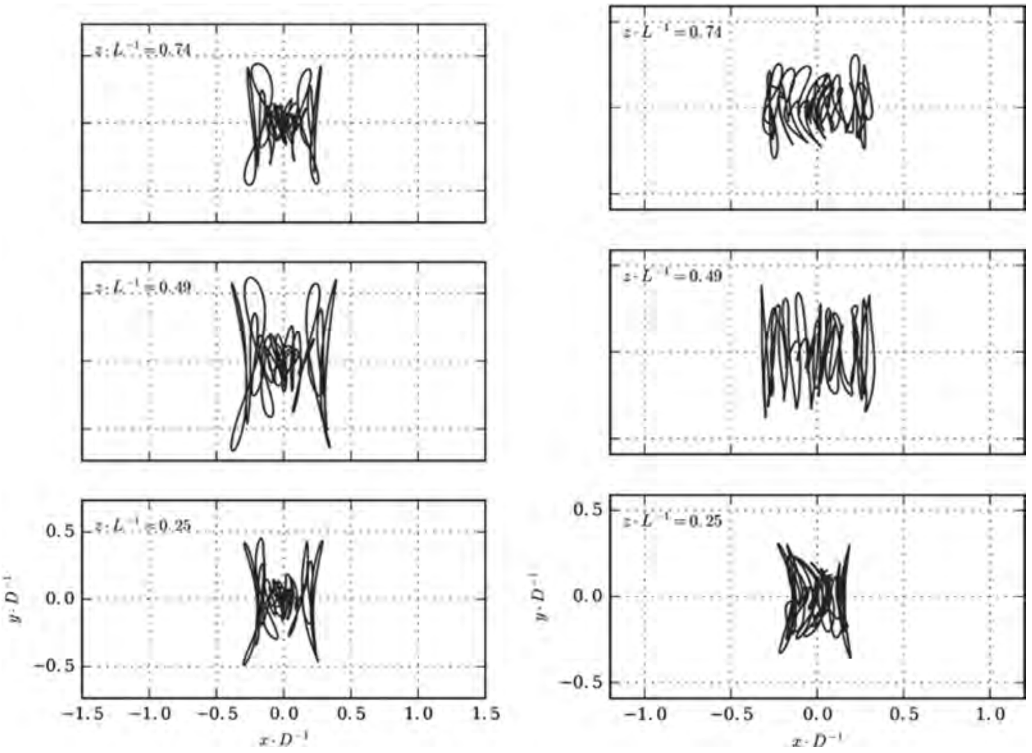

Fig. 11. Relative trajectories of the vibrations of the riser in cases 1 (left) and 3 (right).

with excitation amplitudes in the other direction. In all the simulations excited in both directions, risers move upwards in the cross-flow direction when passing the intersections ('X') of the actual '∞' trajectories. Near the intersections are the high-speed periods and consequently large drag forces, causing large deflections in the opposite directions of support motion. High speeds also mean more intense vibrations in the locally cross-flow direction, forming the lower 'crab plier' shaped parts. Thus the two 'crab plier'-like parts in Figs. 12(b and c) correspond to the 'X' parts in Figs. 13(b and c)

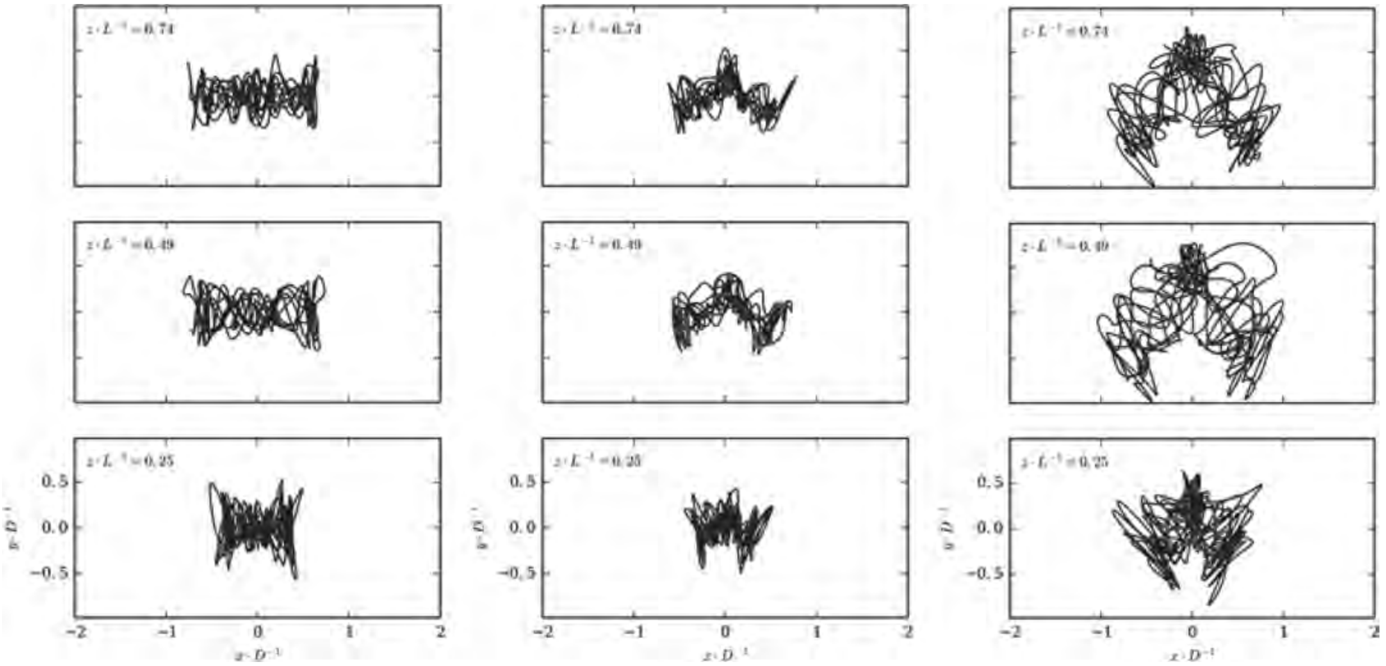

Fig. 12. Relative trajectories of the vibrations of the riser in cases 4 (left), 5 (middle), and 6 (right).

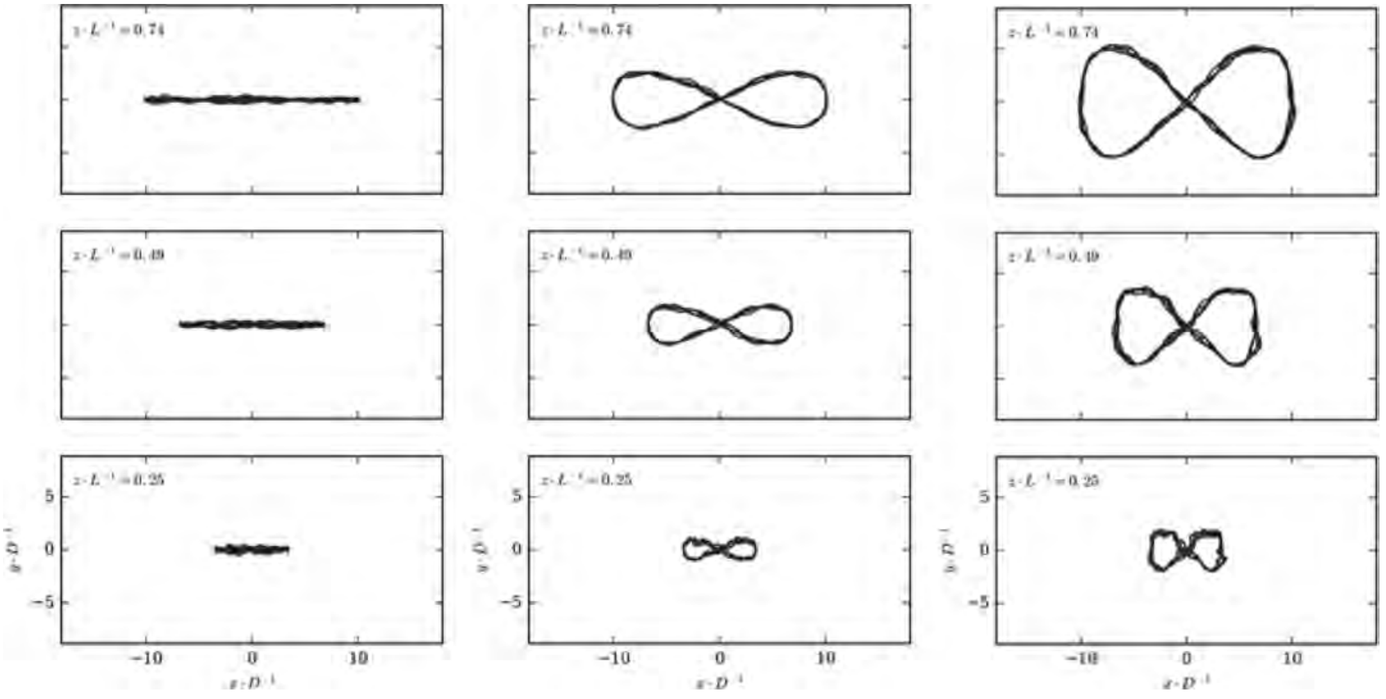

Fig. 13. Actual trajectories of the vibrations of the riser in cases 4 (left), 5 (middle), and 6 (right).

while the top-end knots in Figs. 12(b and c) correspond to two sides in Figs. 13(b and c), the zero in-line excitation velocity periods. Some more complex trajectories may be formed when the phase difference between excitations in two directions becomes non-zero or when the frequency relationship of excitations varies.

Time series of modal weights of the in-line and cross-flow displacements are presented in Figs. 14 and 15, respectively. It is clear that the excitations in the cross-flow direction will influence the in-line displacement for that the actual vortex shedding direction has been changed, indicating that the so-called ‘in-line’ and ‘cross-flow’ directions lost their original meanings. Both drag and lift forces will contribute to the ‘in-line’ and ‘cross-flow’ vibrations. The intensified high-frequency components for case 6 in Fig. 14 can be attributed to the increase in the lift force components and

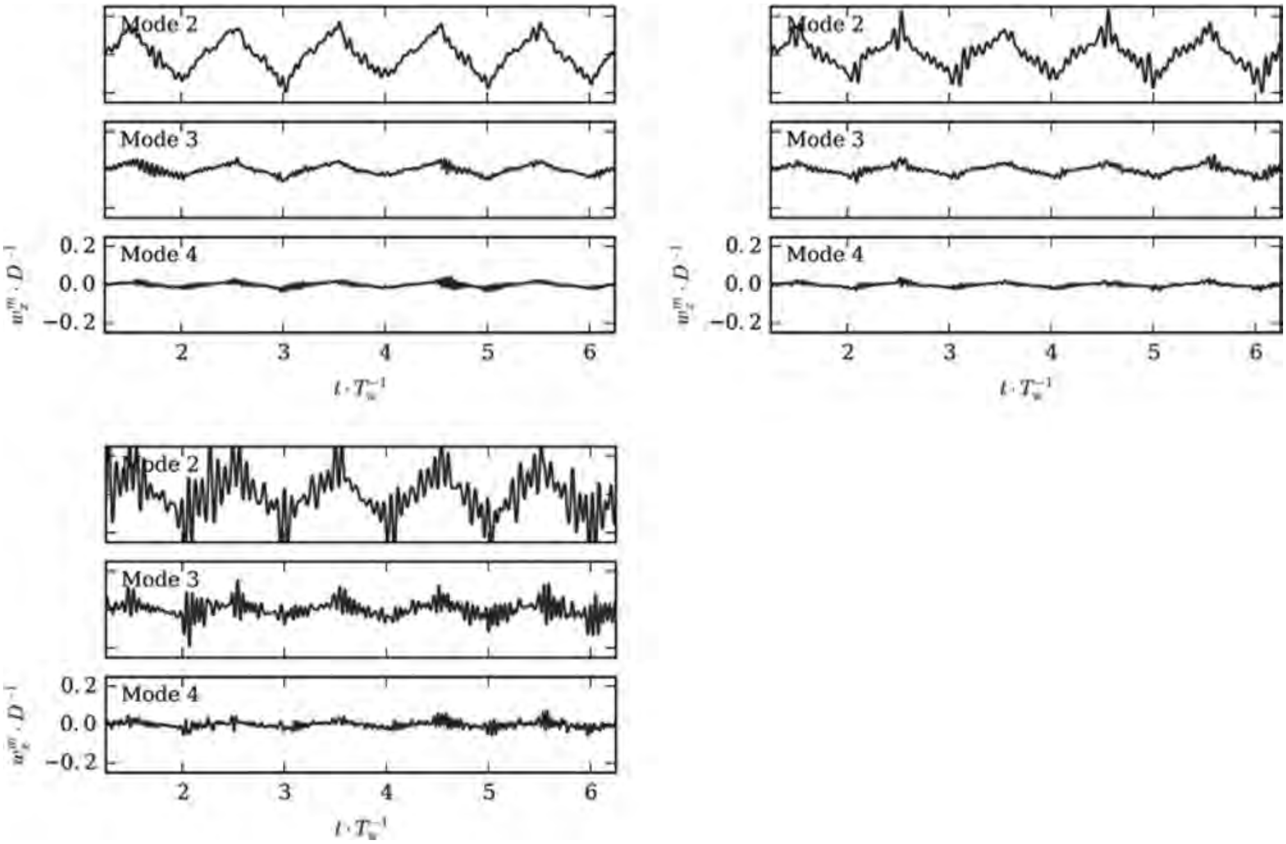

Fig. 14. Time series of modal weights of the in-line displacements $x \cdot D^{-1}$ in cases 4 (left), 5 (middle), and 6 (right), $w_x^m \cdot D^{-1}$.

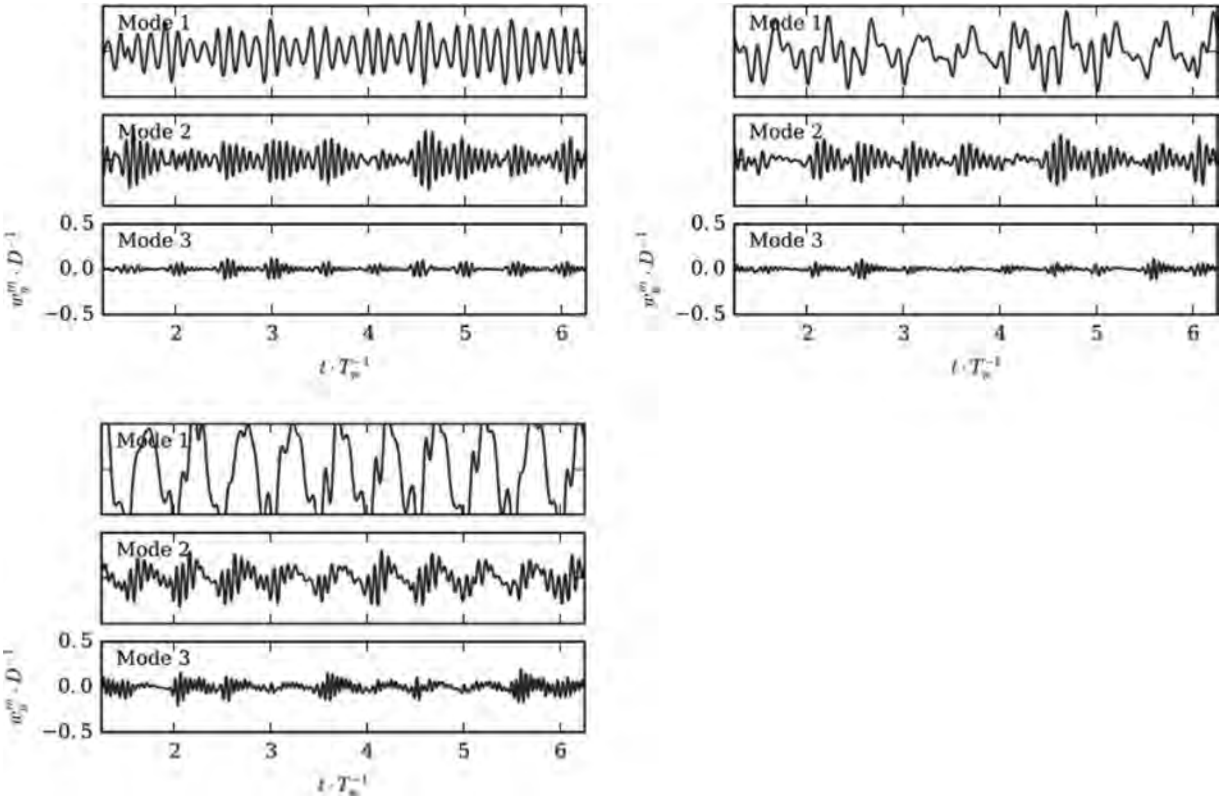

Fig. 15. Time series of modal weights of the cross-flow displacements $y \cdot D^{-1}$ in cases 4 (left), 5 (middle), and 6 (right), $w_y^m \cdot D^{-1}$.

also the decrease in the drag force components in the direction. The vibrations in both directions become quite similar when the cross-flow excitation amplitude is large such as in case 6. Larger cross-flow excitation amplitudes or reduced velocities also mean larger resultant velocities, rendering more intense vibrations. It is clearly seen from Fig. 15 that the high-frequency component of the 1st modal weight in the cross-flow direction decreases with increasing cross-flow excitation amplitude. This may be due to that the vortex shedding direction gets closer to the cross-flow direction, implying larger low-frequency components and smaller high-frequency components (but higher modes may be excited). The low-frequency components discussed before due to the current speed variation along the span appear in the 2nd or even the 3rd modal weights in both directions in cases 5 and 6.

5. Conclusions

Numerical simulations of a vertical riser subject to one-direction or two-direction sinusoidal excitations at its top end in still water have been conducted. The in-line vibrations are found to consist of three components at low reduced velocities, the low-frequency oscillation due to the support motion, the first-natural-frequency vibration during the riser reversal, and the second-natural-frequency vibration due to vortex shedding. The current speed variations along the span when the riser is excited at its top end can cause low-frequency oscillations at higher modes in the excitation direction. This low-frequency oscillation may cause different phase differences between the in-line and cross-flow displacements, and consequently form various trajectories at different positions along the span when the riser is only excited in one direction. More complex trajectories are observed when the riser is excited in two directions.

Acknowledgments

This work is supported by the National Natural Science Foundation of China (51490675, 51379125, 11432009, 51579145), Chang Jiang Scholars Program (T2014099), Shanghai Excellent Academic Leaders Program (17XD1402300), Program for Professor of Special Appointment (Eastern Scholar) at Shanghai Institutions of Higher Learning (2013022), Innovative Special Project of Numerical Tank of Ministry of Industry and Information Technology of China (2016-23/09) and Lloyd's Register Foundation for doctoral student, to which the authors are most grateful.

References

[1] A. Kozakiewicz, B.M. Sumer, J. Fredsøe, J. Waterw. Port Coastal Ocean Eng. 120 (1994) 515–534, doi:10.1061/(ASCE)0733-950X(1996)122:3(155).
[2] B.M. Sumer, J. Fredsøe, J. Offshore Mech. Arct. Eng. 110 (1988) 387–394.
[3] B.M. Sumer, J. Fredsøe, Hydrodynamics Around Cylindrical Structures, World Scientific, Singapore, 1997.
[4] M. Zhao, J. Fluids Struct. 39 (2013) 41–59, doi:10.1016/j.jfluidstructs.2013.02.003.
[5] M. Zhao, K. Kaja, Y. Xiang, G. Yan, Ocean Eng. 73 (2013) 83–95, doi:10.1016/j.oceaneng.2013.08.006.
[6] A.C. Fernandes, S. Mirzaeisefat, L.V. Cascão, Appl. Ocean Res. 47 (2014) 183–191, doi:10.1016/j.apor.2014.04.003.
[7] A.S. Duggal, J.M. Niedzwecki, J. Offshore Mech. Arct. Eng. 117 (1995) 99–104.
[8] P. Anagnostopoulos, G. Iliadis, J. Fluids Struct. 12 (1998) 225–258, doi:10.1006/jfls.1997.0139.
[9] H.I. Park, Y.P. Hong, M. Nakamura, W. Koterayama, in: Proceedings of The Twelfth (2002) International Offshore and Polar Engineering Conference. International Society of Offshore and Polar Engineers, Kitakyushu, Japan, 2002, pp. 199–206.
[10] H.I. Park, Y.P. Hong, M. Nakamura, W. Koterayama, J. Waterw. Port Coastal Ocean Eng. 130 (2004) 207–214, doi:10.1061/(ASCE)0733-950X(2004)130:4(207).
[11] H. Senga, W. Koterayama, Int. J. Offshore Polar Eng. 15 (2005) 274–281.
[12] C.A. Riveros, T. Utsunomiya, K. Maeda, K. Itoh, Int. J. Offshore Polar Eng. 19 (2009) 23–30.
[13] S. Fu, J. Wang, R. Baarholm, J. Wu, C.M. Larsen, J. Offshore Mech. Arct. Eng. 136 (2014) 11801, doi:10.1115/1.4025759.
[14] J. Wang, S. Fu, Y. Xu, L. Song, Chin. J. Theor. Appl. Mech. 46 (2014) 173–182, doi:10.6052/0459-1879-13-277.
[15] M.J. Thorsen, S. Sævik, C.M. Larsen, J. Fluids Struct. 61 (2016) 1–19, doi:10.1016/j.jfluidstructs.2015.11.006.
[16] M. Duan, D. Wan, H. Xue, in: Proceedings of the Twenty-Sixth (2016) International Ocean and Polar Engineering Conference. International Society of Offshore and Polar Engineers (ISOPE), Rhodes, Greece, 2016, pp. 1065–1107.
[17] B. Fu, M. Duan, D. Wan, in: Proceedings of the Second Conference of Global Chinese Scholars on Hydrodynamics Effect, Wuxi, China, 2016, pp. 431–435.
[18] R.H.J. Willden, J.M.R. Graham, Eur. J. Mech. B 23 (2004) 209–218, doi:10.1016/j.euromechflu.2003.09.011.
[19] R.W. Clough, J. Penzien, Dynamics of Structures, third ed., Computers & Structures, Inc., Berkeley, 2003.
[20] H. Jasak, in: Proceedings of the 47th AIAA Aerospace Sciences Meeting Including The New Horizons Forum and Aerospace Exposition, Orlando, Florida, American Institute of Aeronautics and Astronautics, Inc., 2009, doi:10.2514/6.2009-341.
[21] H. Lie, K.E. Kaasen, J. Fluids Struct. 22 (2006) 557–575, doi:10.1016/j.jfluidstructs.2006.01.002.
[22] A.D. Trim, H. Braaten, H. Lie, M.A. Tognarelli, J. Fluids Struct. 21 (2005) 335–361, doi:10.1016/j.jfluidstructs.2005.07.014.